Exciton-polariton mediated light propagation in anisotropic waveguides

Hiroyuki Takeda[1] and Kazuaki Sakoda[2,3]

[1]*International Center for Young Scientists (ICYS), National Institute for Materials Science (NIMS), 1-2-1 Sengen, Tsukuba, Ibaraki 305-0047, Japan*

[2]*Photonic Materials Unit, National Institute for Materials Science (NIMS), 1-1 Namiki, Tsukuba, Ibaraki 305-0044, Japan*

[3]*Graduate School of Pure and Applied Science, University of Tsukuba, 1-1-1 Tennodai, Tsukuba, Ibaraki 305-8571, Japan*

(Received 10 July 2012; revised manuscript received 7 November 2012; published 26 November 2012)

To analyze the exciton-polariton dispersion relation of highly anisotropic thiacyanine films and nanofibers, we formulated a plane-wave expansion method by which we could obtain the eigenfrequencies of polaritons as eigenvalues of a non-Hermitian and frequency-independent matrix. The group refractive index calculated from the slope of the dispersion curve agreed quite well with the Fabry-Perot interference patterns found in both the calculated and observed transmission spectra. We found that the dispersion relation of the anisotropic polariton was quite different from the isotropic case and depended strongly on the tilt angle of the optical transition dipole moment of the constituent molecules to the propagation direction. Material parameters such as the transverse and longitudinal exciton frequencies are also discussed.

DOI: 10.1103/PhysRevB.86.205319 PACS number(s): 71.36.+c, 42.82.Et, 78.66.Qn

I. INTRODUCTION

Optical waveguides are widely used in various fields of science and technology. In conventional waveguides like core/clad optical fibers, the wave propagation is achieved by index guiding, i.e., total reflection due to the higher refractive index of the core material.[1] Because the index difference between the core and clad is usually small, a large bending loss takes place when the optical fiber is bent at a large angle.

The bending loss can be reduced by several means. High-index core materials like silicon apparently reduce the bending loss, while coupled-resonator optical waveguides (CROWs)[2] and photonic-crystal waveguides[3] may give an ultimate solution to this problem although their fabrication cost is very high for optical frequencies. Plasmonic waveguides are another solution for reducing the bending loss,[4] since their wave propagation is achieved by surface plasmons whose electromagnetic field is naturally localized on metal surfaces due to their negative dielectric constants. However, the considerably large dielectric loss of metallic materials at optical frequencies is a general problem for plasmonic waveguides.

Recently, Takazawa presented another promising method. He observed the propagation of optical waves in thiacyanine nanofibers whose dimension was typically 500 nm in diameter and 100 μm in length, and found that the intensity of transmitted waves did not decrease appreciably even when the nanofibers were bent with a radius of curvature as small as 10 μm.[5–7] It was apparent that this small bending loss was not brought about by index guiding. He pointed out the possibility of wave propagation by exciton polaritons, which was later examined theoretically.[8]

Exciton polaritons, which are combined states of excitons and the electromagnetic field, have been studied for a long time.[9–11] In the case of organic systems like aggregates and fibers of thiacyanine molecules, the exciton is of the Frenkel type, that is, both an electron in an excited state and a hole are located in the same molecule and the exciton propagates resonantly from molecule to molecule. Its binding energy is generally large compared with Wannier excitons and their LT splitting (energy difference between the longitudinal and transverse excitons) is also large because of large transition dipole moments of organic dye molecules. These properties stabilize the exciton polaritons even at room temperature.

On the other hand, because exciton polaritons in certain semiconductors such as ZnO are also stable at room temperature,[12–15] their nanowires have been actively studied as efficient optical waveguides in which light is confined more effectively than conventional dielectric waveguides.[16,17]

For bulk exciton polaritons with isotropic dielectric constants, their dispersion relation consists of two branches. The upper branch is located above the longitudinal exciton frequency ω_L, while the lower one is located under the transverse exciton frequency ω_T. There is no eigenmode in the frequency range between them where the dielectric constant is negative. When the frequency of the lower-branch polariton approaches ω_T, its group velocity, which is given by the slope of the dispersion curve, becomes small and its wave number diverges. In the case of polariton waveguides, we should note the presence of the light line defined by the dispersion relation of surrounding materials, above which the electromagnetic modes are leaky. So, those polariton modes with large wave numbers, which are far from the light line, are expected to be tolerant of the leakage on waveguide corners.

In addition to Refs. 5–8, stable propagation and lasing of exciton polaritons at room temperature have been reported in several organic crystals.[18–21] When we analyze the polariton modes in these organic crystals, we have to take into consideration the large anisotropy of their optical response, since their transition dipole moments are aligned in certain crystallographic directions. For example, in J (H) aggregates, the transition dipole moments of adjacent molecules are aligned side-by-side (face-to-face) to result in a red (blue) shift of their absorption band from their monomer absorption.[22] In the case of polariton nanofibers, the tilt angle α of the transition dipole moment to the fiber axis was regarded as $0^\circ \leqslant \alpha \leqslant 54.7^\circ$ for J aggregates and $54.7^\circ < \alpha \leqslant 90^\circ$ for H aggregates based on the point-dipole approximation.[22] $\alpha = 0^\circ$ and 90° are often chosen as ideal values for J and H aggregates, respectively. Although these aggregates have long been studied

by many researchers, their properties as optical waveguides are still unclear.

In this paper, we reexamine the polariton states of thiacyanine waveguides by fully taking into account the anisotropy of their dielectric constant, which results in dispersion curves qualitatively different from those reported in Ref. 8. In many crystalline organic systems including thiacyanine nanofibers, their dielectric constant is highly anisotropic due to the anisotropy of their molecular structure and orientation in the crystal. In the present case of thiacyanine nanofibers, the tilt angle of molecules to the fiber axis is unknown so far. We will determine it by comparing our calculation with observation provided by Takazawa. This information of the tilt angle will then be used to fix the anisotropic dielectric tensor that will be used in successive calculations.

This paper is organized as follows. In Sec. II, we derive the anisotropic dielectric tensor of nanofibers assuming a uniform tilt angle of thiacyanine molecules to the fiber axis. We also formulate a plane-wave expansion (PWE) method to calculate the dispersion relation for the thiacyanine nanofiber and film. We further derive basic equations for the finite-difference time-domain (FDTD) calculation of the wave propagation. In Sec. III, we present the numerical results of dispersion curves for four different tilt angles calculated by the PWE method and transmission spectra calculated by the FDTD method. We show that the group refractive index derived from these two methods agree with each other quite well, which proves the accuracy of our calculation. We also show a good agreement between our calculation and the group refractive index reported in Takazawa's experiments.[8] A brief summary of the present study is given in Sec. IV. In Appendix A, a key equation is derived for the non-Hermitian eigenproblem of the present study. An important feature of the anisotropic dielectric tensor, which results in an infinite number of dispersion curves, is described in Appendix B.

II. THEORY

In this section, we derive the anisotropic frequency-dependent dielectric tensor of exciton polaritons and discuss the computational methods for dispersion curves and light propagation.

A. Anisotropic dielectric tensor

In the Hamiltonian $\mathcal{H}$, we consider N identical two-level systems with ground and excited states:

$$\mathcal{H} = \frac{\hbar\omega_0}{2} J_3 - \mathbf{d}_0 \cdot \mathbf{E}(t)\,[J_{12} + J_{21}]\,, \tag{1}$$

where ω_0 is the transition frequency between the ground and excited states, $\mathbf{d}_0$ is the transition dipole moment, and $\mathbf{E}(t)$ is the electric field. While $J_3 \equiv J_{22} - J_{11}$ denotes the population difference between the two states, J_{12} (J_{21}) deexcites (excites) one two-level system to the ground (excited) state. The atomic operators satisfy $[J_{12}, J_3] = 2J_{12}$, $[J_3, J_{21}] = 2J_{21}$, and $[J_{21}, J_{12}] = J_3$. The Heisenberg equation of motion yields

$$\begin{aligned}\frac{d\langle J_{12}(t)\rangle}{dt} &= -\frac{i}{\hbar}\langle [J_{12}(t), \mathcal{H}]\rangle \\ &= -i\omega_0\langle J_{12}(t)\rangle - i\frac{\mathbf{d}_0 \cdot \mathbf{E}(t)}{\hbar}\langle J_3(t)\rangle,\end{aligned} \tag{2}$$

where brackets denote statistical averages. When the intensity of the electric field is not very high, we can safely assume that $\langle J_3(t)\rangle \simeq -N$. Then, the electric polarization $\mathbf{P}(t) \equiv d_0\mathbf{n}\,[\langle J_{12}(t)\rangle + \langle J_{21}(t)\rangle]\,/\,V$, where $\mathbf{n} \equiv \mathbf{d}_0/d_0$ is a unit vector and V is the volume, satisfies

$$\frac{d^2\mathbf{P}(t)}{dt^2} + \omega_0^2\mathbf{P}(t) = \frac{2\omega_0 N d_0^2}{\hbar V}\,[\mathbf{n} \cdot \mathbf{E}(t)]\,\mathbf{n}. \tag{3}$$

By Fourier transformation of $\mathbf{P}(t)$ with respect to time, we obtain

$$\mathbf{P}(\omega) = \frac{2\omega_0 N d_0^2}{\hbar V\left(\omega_0^2 - \omega^2\right)}\mathbf{n} \otimes \mathbf{n} \cdot \mathbf{E}(\omega), \tag{4}$$

where $(\mathbf{n} \otimes \mathbf{n})_{ij} = n_i n_j$ and $[\mathbf{n} \cdot \mathbf{E}(\omega)]\mathbf{n} = \mathbf{n} \otimes \mathbf{n} \cdot \mathbf{E}(\omega)$. $\mathbf{P}(\omega)$ and $\mathbf{E}(\omega)$ are the frequency components of $\mathbf{P}(t)$ and $\mathbf{E}(t)$, respectively. From $\varepsilon_0\varepsilon_\infty\mathbf{E}(\omega) + \mathbf{P}(\omega) = \varepsilon_0\boldsymbol{\varepsilon}(\omega)\mathbf{E}(\omega)$, where ε_0 is the permittivity in free space and ε_∞ is the dielectric constant at high frequencies, the frequency-dependent dielectric tensor $\boldsymbol{\varepsilon}(\omega)$ is given by

$$\begin{aligned}\boldsymbol{\varepsilon}(\omega) &= \varepsilon_\infty\mathbf{1} + \frac{2\omega_0 N d_0^2}{\varepsilon_0\hbar V\left(\omega_0^2 - \omega^2\right)}\mathbf{n} \otimes \mathbf{n} \\ &= \varepsilon_\infty\left\{\mathbf{1} + 2\frac{\omega_L^2 - \omega_T^2}{\omega_T^2 - \omega^2}\mathbf{n} \otimes \mathbf{n}\right\},\end{aligned} \tag{5}$$

where $\mathbf{1}$ denotes a unit tensor. We have chosen $\omega_T = \omega_0$ and $\omega_L^2 - \omega_T^2 = (\omega_0 N d_0^2)/(\varepsilon_0\varepsilon_\infty\hbar V)$. When transition dipole moments are uniformly aligned in the xz plane, $\mathbf{n} = (\sin\alpha, 0, \cos\alpha)$, where α is the orientation angle to the z axis. Then, the frequency-dependent dielectric tensor is

$$\boldsymbol{\varepsilon}(\omega) = \varepsilon_\infty\left\{\mathbf{1} + 2\frac{\omega_L^2 - \omega_T^2}{\omega_T^2 - \omega^2}\begin{bmatrix}\sin^2\alpha & 0 & \sin\alpha\cos\alpha \\ 0 & 0 & 0 \\ \sin\alpha\cos\alpha & 0 & \cos^2\alpha\end{bmatrix}\right\}. \tag{6}$$

On the other hand, when transition dipole moments are randomly oriented in the xz plane, $\langle\sin^2\alpha\rangle_{av} \equiv (1/2\pi)\int_0^{2\pi} d\alpha\,\sin^2\alpha = 1/2$, $\langle\cos^2\alpha\rangle_{av} = 1/2$, and $\langle\sin\alpha\cos\alpha\rangle_{av} = 0$. (The subscript av denotes the average value.) Then,

$$\boldsymbol{\varepsilon}(\omega) = \varepsilon_\infty\begin{bmatrix}\frac{\omega_L^2 - \omega^2}{\omega_T^2 - \omega^2} & 0 & 0 \\ 0 & 1 & 0 \\ 0 & 0 & \frac{\omega_L^2 - \omega^2}{\omega_T^2 - \omega^2}\end{bmatrix}. \tag{7}$$

B. PWE method for dispersion curves

We calculate the dispersion curves of films and fibers with anisotropic polariton dielectric tensors by the PWE method with a supercell technique. According to the experimental condition of Takazawa *et al.*,[5–8] we assume that a film or a fiber is placed on a transparent glass substrate. We take Cartesian coordinates as shown in Fig. 1. In the case of the polariton film, we denote its height by h and assume that it uniformly occupies all the xz plane. For the polariton fiber, we assume that it has a rectangular cross section and denote its height and width by h and w, respectively. We also assume that it is infinitely long in the z direction. As we mentioned before,

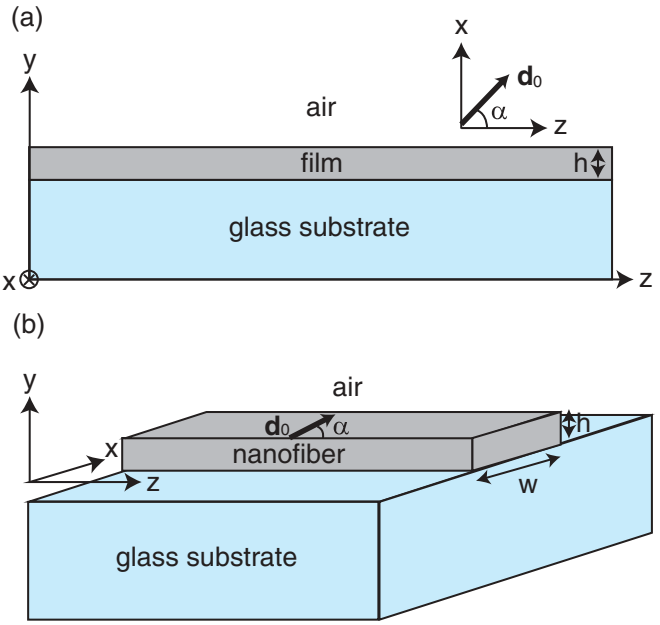

FIG. 1. (Color online) The structures of (a) the polariton film and (b) nanofiber made of crystalline aggregates of thiacyanine molecules that are assumed in our calculation. They are placed on transparent glass (SiO_2) substrates according to the experimental condition by Takazawa. Their dimensions are also chosen according to his observations. It is assumed that the transition dipole moment $\mathbf{d}_0$ of thiacyanine molecules is tilted at angle α to the wave propagation (z) direction in the xz plane.

we further assume that the transition dipole moment of the constituent molecules is tilted from the z axis, which is the direction of wave propagation, by angle α in the xz plane.

To apply the PWE method to the present problem, we have to assume a structural periodicity in the y direction for the film and in both the x and y directions for the fiber, that is, we assume $\varepsilon(y,\omega) = \varepsilon(y + L_y,\omega)$, with a condition of $L_y \gg h$, etc., so that the presence of multiple layers has a negligible influence on the dispersion curves.

By eliminating the magnetic field from the Maxwell equations, the eigenequation for the electric field is obtained as follows:

$$\nabla \times \nabla \times \mathbf{E}_{n\mathbf{k}}(\mathbf{r}) = \frac{\omega_{n\mathbf{k}}^2}{c^2}\boldsymbol{\varepsilon}(\mathbf{r};\omega_{n\mathbf{k}}) \cdot \mathbf{E}_{n\mathbf{k}}(\mathbf{r}), \tag{8}$$

where n is the band index, $\mathbf{k} \equiv (0,0,k_z)$ is the wave vector, and $\omega_{n\mathbf{k}}$ is the eigen-angular-frequency. We should note that the dielectric tensor $\boldsymbol{\varepsilon}$ is dependent on position $\mathbf{r}$ and frequency. We denote it as a sum of frequency-independent and -dependent terms:

$$\boldsymbol{\varepsilon}(\mathbf{r};\omega_{n\mathbf{k}}) = \eta(\mathbf{r})\mathbf{1} + 2\frac{\xi(\mathbf{r})c^2}{\omega_T^2 - \omega_{n\mathbf{k}}^2}\mathbf{n} \otimes \mathbf{n}. \tag{9}$$

From Eq. (6), $\eta(\mathbf{r})$ is ε_∞ in the polariton film and fiber. Otherwise, it is the dielectric constant of the substrate or air. $\xi(\mathbf{r}) = \varepsilon_\infty(\omega_L^2 - \omega_T^2)/c^2$ in the film or fiber, and $\xi(\mathbf{r}) = 0$ otherwise. Because $\eta(\mathbf{r})$ and $\xi(\mathbf{r})$ are periodic functions according to the supercell condition, they can be expressed by Fourier series:

$$\eta(\mathbf{r}) = \sum_{\mathbf{G}} \eta_{\mathbf{G}} e^{i\mathbf{G}\cdot\mathbf{r}}, \tag{10}$$

$$\xi(\mathbf{r}) = \sum_{\mathbf{G}} \xi_{\mathbf{G}} e^{i\mathbf{G}\cdot\mathbf{r}}, \tag{11}$$

where $\mathbf{G}$ is the reciprocal lattice vector, which is given by $\mathbf{G} = (0, 2\pi m_y/L_y, 0)$ for the film and $\mathbf{G} = (2\pi m_x/L_x, 2\pi m_y/L_y, 0)$ for the fiber, where m_x and m_y are integers. In the actual numerical calculation, we have to truncate the infinite summation for m_x and m_y in Eqs. (10) and (11) at sufficiently large values, which we denote by M_x and M_y. So, we take $|m_x| \leqslant M_x$ and $|m_y| \leqslant M_y$. Then, the number of reciprocal lattice vectors taken into consideration, $N_{\mathbf{G}}$, is $2M_y + 1$ for the film and $(2M_x + 1)(2M_y + 1)$ for the fiber.

Taking the electric flux density $\mathbf{D}_{n\mathbf{k}}(\mathbf{r}) = \varepsilon_0\boldsymbol{\varepsilon}(\mathbf{r};\omega_{n\mathbf{k}}) \cdot \mathbf{E}_{n\mathbf{k}}(\mathbf{r}) = \varepsilon_0\eta(\mathbf{r})\mathbf{E}_{n\mathbf{k}}(\mathbf{r}) + \mathbf{P}_{n\mathbf{k}}(\mathbf{r})$, where $\mathbf{P}_{n\mathbf{k}}(\mathbf{r}) = 2\varepsilon_0\xi(\mathbf{r})c^2\mathbf{n} \otimes \mathbf{n} \cdot \mathbf{E}_{n\mathbf{k}}(\mathbf{r})/(\omega_T^2 - \omega_{n\mathbf{k}}^2) = 2\varepsilon_0\xi(\mathbf{r})c^2\,[\mathbf{n} \cdot \mathbf{E}_{n\mathbf{k}}(\mathbf{r})]\,\mathbf{n}/(\omega_T^2 - \omega_{n\mathbf{k}}^2)$, Eq. (8) is decomposed into two equations:

$$\nabla \times \nabla \times \eta^{-1}(\mathbf{r})\mathbf{D}_{n\mathbf{k}}(\mathbf{r}) - \nabla \times \nabla \times \eta^{-1}(\mathbf{r})\mathbf{P}_{n\mathbf{k}}(\mathbf{r}) = \frac{\omega_{n\mathbf{k}}^2}{c^2}\mathbf{D}_{n\mathbf{k}}(\mathbf{r}), \tag{12}$$

$$-2\xi(\mathbf{r})\eta^{-1}(\mathbf{r})\,[\mathbf{n} \cdot \mathbf{D}_{n\mathbf{k}}(\mathbf{r})]\,\mathbf{n} + \frac{\omega_T^2}{c^2}\mathbf{P}_{n\mathbf{k}}(\mathbf{r}) + 2\xi(\mathbf{r})\eta^{-1}(\mathbf{r})\,[\mathbf{n} \cdot \mathbf{P}_{n\mathbf{k}}(\mathbf{r})]\,\mathbf{n} = \frac{\omega_{n\mathbf{k}}^2}{c^2}\mathbf{P}_{n\mathbf{k}}(\mathbf{r}). \tag{13}$$

We have used $\varepsilon_0\mathbf{E}_{n\mathbf{k}}(\mathbf{r}) = \eta^{-1}(\mathbf{r})[\mathbf{D}_{n\mathbf{k}}(\mathbf{r}) - \mathbf{P}_{n\mathbf{k}}(\mathbf{r})]$. From Bloch's theorem,

$$\mathbf{D}_{n\mathbf{k}}(\mathbf{r}) = \sum_{\mathbf{G}}\sum_{\lambda=1}^{2} D_{n\mathbf{k}}^{(\lambda)}(\mathbf{G})\mathbf{e}_{\mathbf{k}+\mathbf{G}}^{(\lambda)} e^{i(\mathbf{k}+\mathbf{G})\cdot\mathbf{r}}, \tag{14}$$

$$\mathbf{P}_{n\mathbf{k}}(\mathbf{r}) = \sum_{\mathbf{G}} P_{n\mathbf{k}}(\mathbf{G}) e^{i(\mathbf{k}+\mathbf{G})\cdot\mathbf{r}}\mathbf{n}, \tag{15}$$

where $e_{\mathbf{k}+\mathbf{G}}^{(1)}$ and $e_{\mathbf{k}+\mathbf{G}}^{(2)}$ are unit vectors perpendicular to $\mathbf{k} + \mathbf{G}$. We assume without loss of generality that $e_{\mathbf{k}+\mathbf{G}}^{(1)}$, $e_{\mathbf{k}+\mathbf{G}}^{(2)}$, and $\mathbf{k} + \mathbf{G}$ form a right-handed orthogonal system. Then, it follows that $\nabla \cdot \mathbf{D}_{n\mathbf{k}}(\mathbf{r}) = 0$ as it should be. As described in Sec. II A, we should also note that $\mathbf{P}_{n\mathbf{k}}(\mathbf{r})$ is parallel to $\mathbf{n}$. Substituting Eqs. (10), (11), (14), and (15) into Eqs. (12) and (13), we obtain the following $3N_{\mathbf{G}}$-dimensional non-Hermitian eigenvalue equation (Appendix A):

$$\begin{bmatrix} \mathbf{M}_{DD}^{(\mathbf{k})} & \mathbf{M}_{DP}^{(\mathbf{k})} \\ \mathbf{M}_{PD}^{(\mathbf{k})} & \mathbf{M}_{PP}^{(\mathbf{k})} \end{bmatrix} \begin{bmatrix} \tilde{\mathbf{D}}_{n\mathbf{k}} \\ \tilde{\mathbf{P}}_{n\mathbf{k}} \end{bmatrix} = \frac{\omega_{n\mathbf{k}}^2}{c^2} \begin{bmatrix} \tilde{\mathbf{D}}_{n\mathbf{k}} \\ \tilde{\mathbf{P}}_{n\mathbf{k}} \end{bmatrix}, \tag{16}$$

where $\tilde{\mathbf{D}}_{n\mathbf{k}}$ and $\tilde{\mathbf{P}}_{n\mathbf{k}}$ are $2N_{\mathbf{G}}$- and $N_{\mathbf{G}}$-dimensional vectors, respectively, in which the $\mathbf{G}$ elements are $[D_{n\mathbf{k}}^{(1)}(\mathbf{G}), D_{n\mathbf{k}}^{(2)}(\mathbf{G})]$ and $P_{n\mathbf{k}}(\mathbf{G})$ and $\mathbf{M}_{DD}^{(\mathbf{k})}$, $\mathbf{M}_{DP}^{(\mathbf{k})}$, $\mathbf{M}_{PD}^{(\mathbf{k})}$, and $\mathbf{M}_{PP}^{(\mathbf{k})}$ are $2N_{\mathbf{G}} \times 2N_{\mathbf{G}}$, $2N_{\mathbf{G}} \times N_{\mathbf{G}}$, $N_{\mathbf{G}} \times 2N_{\mathbf{G}}$, and $N_{\mathbf{G}} \times N_{\mathbf{G}}$ matrices, respectively.

C. FDTD method for wave propagation

The electric field $\mathbf{E}(\mathbf{r},t)$ and magnetic field $\mathbf{H}(\mathbf{r},t)$ satisfy the Maxwell equations:

$$\nabla \times \mathbf{E}(\mathbf{r},t) = -\mu_0\frac{\partial \mathbf{H}(\mathbf{r},t)}{\partial t}, \tag{17}$$

$$\nabla \times \mathbf{H}(\mathbf{r},t) = \frac{\partial \mathbf{P}(\mathbf{r},t)}{\partial t} + \varepsilon_0\eta(\mathbf{r})\frac{\partial \mathbf{E}(\mathbf{r},t)}{\partial t}, \tag{18}$$

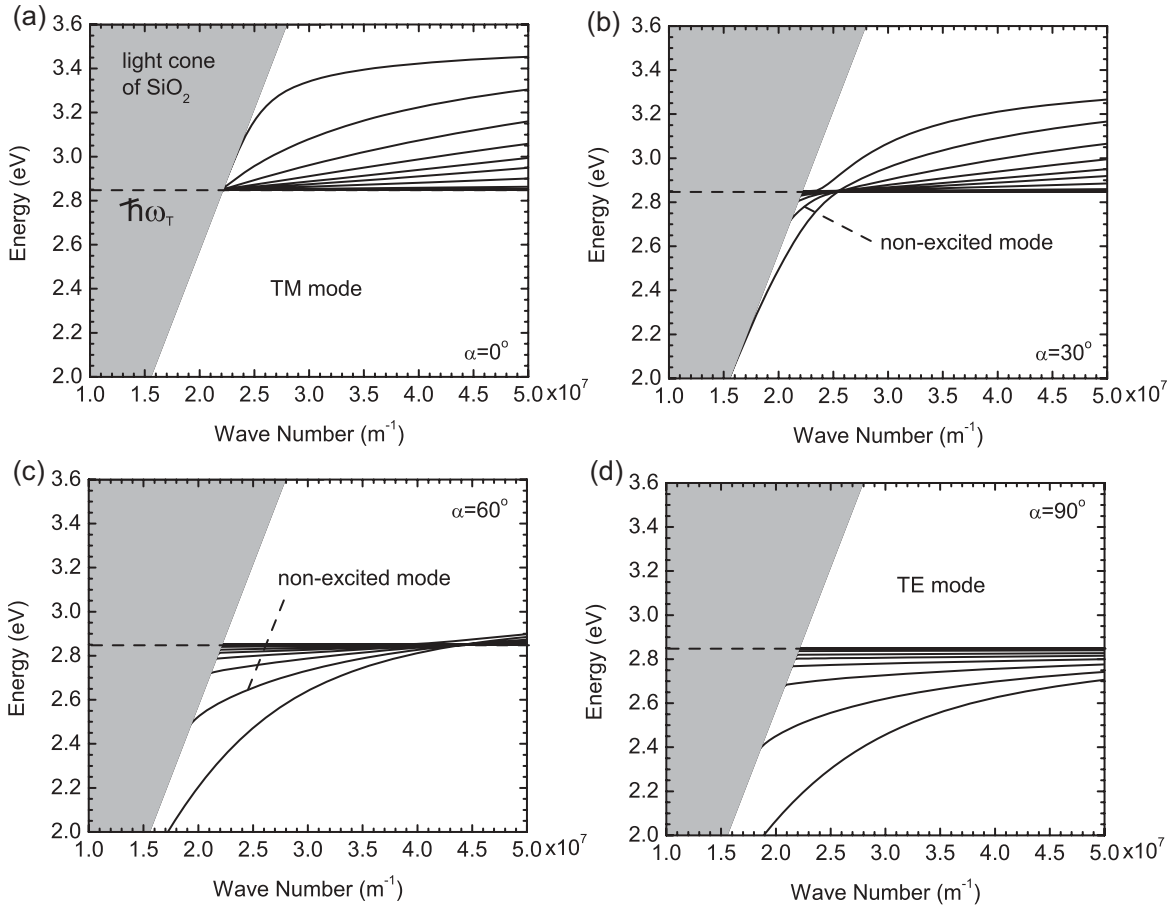

FIG. 2. Dispersion curves of exciton polaritons for (a) $\alpha = 0^\circ$, (b) 30°, (c) 60°, and (d) 90° in the thiacyanine film on a glass substrate. Gray regions are light cones in which electromagnetic modes are leaky. Dispersion curves for $\alpha = 0^\circ$ and 90° are TM and TE modes, respectively.

where μ_0 is the permeability in free space. From Eq. (3), $\mathbf{P}(\mathbf{r},t)$ in films and nanofibers satisfies

$$\frac{d^2\mathbf{P}(\mathbf{r},t)}{dt^2} + \omega_T^2\mathbf{P}(\mathbf{r},t) = 2\varepsilon_0\varepsilon_\infty\left(\omega_L^2 - \omega_T^2\right)[\mathbf{n}\cdot\mathbf{E}(\mathbf{r},t)]\,\mathbf{n}. \tag{19}$$

Otherwise, $\mathbf{P}(\mathbf{r},t) = 0$. Solving Eqs. (17), (18), and (19) self-consistently, time-dependent light propagation can be obtained. In the FDTD method, these equations are discretized with respect to time and space. On the boundary of the computational domain, the second-order Higdon absorbing boundary condition is used to enable electromagnetic waves to propagate without reflection.[23]

III. Results and discussion

A. Material parameters

For numerical calculation of dispersion curves and wave propagation, we need several material parameters. For transverse and longitudinal exciton frequencies, we use $\hbar\omega_T = 2.85$ eV and $\hbar\omega_L = 3.2$ eV, which were obtained from observed reflection spectra as described in Sec. III D. On the other hand, we take $h = 150$ nm and $w = 500$ nm in Fig. 1 as representative values obtained by experimental studies by Takazawa.[5–8] For dielectric constants, we use $\varepsilon_{\mathrm{SiO_2}} = 2.34$ and $\varepsilon_{\mathrm{air}} = 1.0$, respectively. As for ε_∞ of thiacyanine films and nanofibers, it is unknown so far. However, it does not affect numerical results much, so we assume the same value for it as SiO_2, i.e., 2.34.

B. Numerical results for films

When we ignore the spatial dispersion, conventional isotropic bulk exciton polaritons have the dispersion relation $k = (\omega/c)\sqrt{\varepsilon(\omega)} > 0$, where $\varepsilon(\omega) = \varepsilon_\infty(\omega_L^2 - \omega^2)/(\omega_T^2 - \omega^2)$. Thus, while there exist lower and upper branches for $\omega < \omega_T$ and $\omega > \omega_L$, respectively, an exciton-polariton gap appears for $\omega_T \leqslant \omega \leqslant \omega_L$. For $\omega < \omega_T$, the wave number diverges as ω approaches ω_T.

The dispersion relation is very different for exciton polaritons in anisotropic films. Figure 2 shows dispersion curves calculated by the PWE method for four different tilt angles. Gray areas, which are separated from lower regions by the light line $\omega = ck/\sqrt{\varepsilon_{\mathrm{SiO_2}}}$, denote light cones where electromagnetic modes are leaky. Genuine eigenmodes are shown by solid lines under the light line. For this calculation, we took $L_y = 2.0\ \mu$m and $N_{\mathbf{G}} = 81$ and we placed the thiacyanine film in the center of the supercell. We checked the convergence of the calculation by increasing L_y and $N_{\mathbf{G}}$ and confirmed that no appreciable changes took place in the dispersion curves except their number.

As is shown in Appendix B, there are an infinite number of dispersion curves for exciton polariton films with anisotropic dielectric tensors. The number of dispersion curves found by our PWE method with the supercell approximation is, however, limited by the number of plane waves used in the calculation, $N_{\mathbf{G}}$. In each panel of Fig. 2, the first ten dispersion curves are plotted. We should note that this feature of multiple dispersion curves is distinct from coupled surface polaritons in isotropic thin films. In the latter case, there is one surface polariton branch on each of the two surfaces in the frequency range of $\omega_T < \omega < \omega_L$, and when the thickness of the film is sufficiently small, two surface polariton branches are mixed to generate symmetric and antisymmetric coupled surface polaritons.

The dispersion curves strongly depend on the tilt angle α of the transition dipole moment in the film. When off-diagonal elements of the dielectric tensor vanish in Eq. (6), which happens for $\alpha = 0^\circ$ and 90°, polaritons can be classified into TM (transverse magnetic) modes, for which $\alpha = 0^\circ$ and the magnetic (electric) field is parallel to the x axis (yz plane), and TE (transverse electric) modes for which $\alpha = 90^\circ$ and the electric (magnetic) field is parallel to the x axis (yz plane). This classification, however, does not apply to general α. As α increases from 0° to 90°, dispersion curves move from $\omega > \omega_T$ to $\omega < \omega_T$ and the lowest dispersion curve becomes especially distant from the light line.

For long-distance light propagation with clear Fabry-Perot interference as observed in experiments,[8] a frequency region of single-mode propagation is necessary. By this condition, we can restrict the range of possible α. For example, there is no such frequency region in Fig. 2(a), so the possibility of $\alpha = 0^\circ$ can be eliminated. In each of the remaining three cases, there is a single-mode range in the low frequency region. In addition, there is an interesting feature for the second lowest branch in panels (b) and (c), which results in an effectively wider single-mode frequency range. In the experimental study of Takazawa, optical transmittance was measured with fluorescence of thiacyanine molecules in the specimens as a light source. So, its electric field is polarized in the xz plane. On the other hand, we found that the dominant component of the electric field of the second lowest branch is perpendicular to the xz plane. Therefore, the coupling between them is small and clear single-mode Fabry-Perot interference by the lowest mode is expected even in the frequency range of the second lowest mode. Such a single-mode propagation range is $\hbar\omega < 2.82$ eV for $\alpha = 30^\circ$ and $\hbar\omega < 2.72$ eV for $\alpha = 60^\circ$.

In order to verify the above discussion, we calculated the Fabry-Perot peaks for $\alpha = 30^\circ$ and 60° in films with a propagation length of 5 μm by the FDTD method (Sec. II C). In Fig. 1(a), space and time were discretized such that $\Delta y/a = 1/20$, $\Delta z/a = 1/60$, and $c\Delta t/a = 1/120$, respectively, where $a = 500$ nm. Since we have to deal with large k_z and the wavelength in the z direction becomes very short, we had to take a finer mesh in the z direction than in the y direction for accurate calculation.

The entire computational domain was $-3.5 \leqslant y \leqslant 1.5$ μm and $|z| \leqslant 3.5$ μm. The region of $|y| \leqslant 75$ nm and $|z| \leqslant 2.5$ μm was occupied by the film, and the region of $y < -75$ nm was occupied by the glass substrate. We excited the left edge of the film by a Gaussian-pulse electric field $\mathbf{E}_{in}(t)$ polarized parallel to $\mathbf{d}_0$ with a center frequency $\hbar\omega$ of 2.5 eV and a full width at half maximum of 0.3 eV. The output electric field $\mathbf{E}_{\text{out}}(t)$ was evaluated by an average on the right edge of the film: $\mathbf{E}_{\text{out}}(t) \equiv 1/h \int_{-h/2}^{h/2} dy \mathbf{E}(y,t)$.

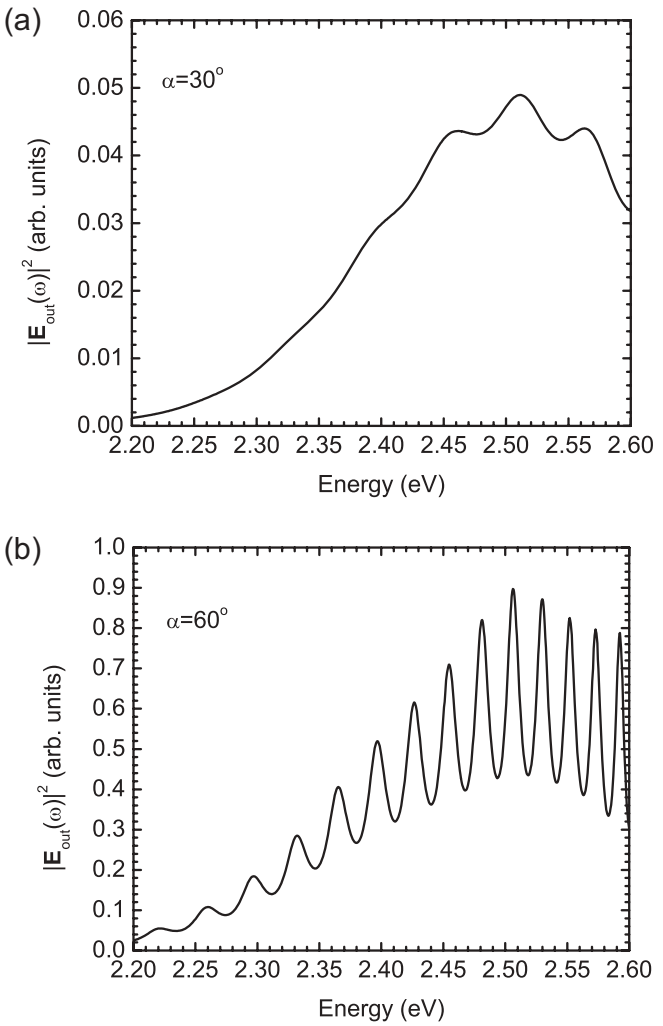

FIG. 3. Transmission spectra of the thiacyanine film for (a) $\alpha = 30^\circ$ and (b) 60°.

Figure 3 shows transmission spectra thus calculated for $\alpha = 30^\circ$ and 60°, where Fabry-Perot interference peaks are observed. The transmission intensity was scaled with the fluorescence intensity of thiacyanine specimens, which is shown in Fig. 4, to easily compare with experimental observations. Figure 4 shows experimental results of absorption and fluorescence spectra of the thiacyanine nanofiber (solid line) and monomer (dashed line) in aqueous solution.[5] The inset is the structural formula of thiacyanine. There are two peaks in the absorption spectrum of thiacyanine nanofibers in aqueous solution at approximately 3.1 and 2.95 eV, the latter of which is the same as the monomer solution. In the specimen of the nanofibers in water, there also existed uncrystallized monomers. So, the absorption peak at 2.95 eV was attributed to the monomer absorption. Then, the absorption peak of the nanofiber is blue shifted by 0.15 eV, which is characteristic of H aggregates.[22] The Stokes shift is large,[24] so there is only a small

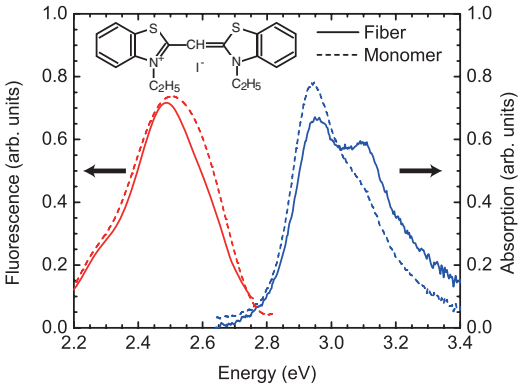

FIG. 4. (Color online) Absorption and fluorescence spectra of thiacyanine fiber (solid line) and monomer (dashed line) in aqueous solution. The inset is the structural formula of thiacyanine. Experimental data were provided by Takazawa.[5]

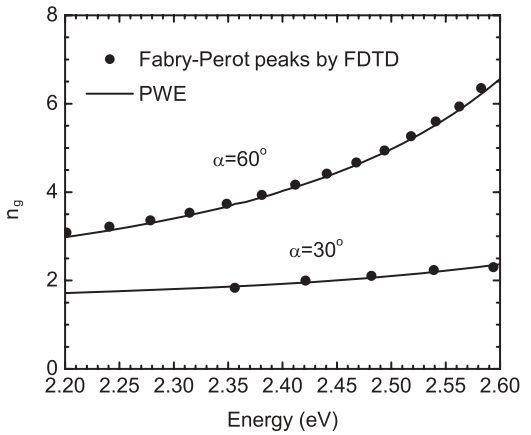

FIG. 5. Group refractive indices of the thiacyanine film calculated by the PWE (solid line) and FDTD (solid circle) methods for $\alpha = 30^\circ$ and 60°.

overlap between the absorption and emission spectra. Details of the fabrication of the nanofibers can be found in Refs. 5,6. In Fig. 3, transmission intensity for $\hbar\omega < 2.6$ eV is shown, since the fluorescence emission is free from reabsorption in this range. As is found in Fig. 2(c), there is the second lowest mode for $\hbar\omega > 2.5$ eV for $\alpha = 60^\circ$. But we still can observe clear monotonic interference peaks between 2.5 and 2.6 eV due to the small coupling between the second lowest mode and the fluorescence emission as mentioned previously. The finesse of the Fabry-Perot interference is larger for $\alpha = 60^\circ$ than $\alpha = 30^\circ$, which originates from a larger group refractive index n_g for the former.

We can evaluate n_g by two methods. Since $n_g \equiv c/v_g \equiv c(\partial\omega/\partial k_z)^{-1}$, where v_g denotes the group velocity in the z direction, we can directly obtain n_g from the dispersion curve calculated by the PWE method. On the other hand, it can also be evaluated from the spacing between interference peaks as follows. When we denote the length of the specimen by L, the condition for achieving peaks in the interference pattern is given by $k_z \times 2L = 2\pi m$, where m is an integer. So, when we denote the frequencies of two successive peaks by ω_m and ω_{m+1}, then $\omega_{m+1} - \omega_m \approx (\partial\omega/\partial k_z)\Delta k_z = \pi v_g/L$. Therefore, $n_g \approx \pi c/[L(\omega_{m+1} - \omega_m)]$. The results are shown in Fig. 5, where a good agreement between the two independent calculations is found. This gives evidence of the accuracy of our calculations.

In Fig. 6, we show the distribution of the electric-field amplitude $|\mathbf{E}(y,z)|$, induced by a continuous excitation with an x-polarized electric field at $\hbar\omega = 2.5925$ eV, which is one of the peak frequencies observed in Fig. 3(b), on the left edge of the film. For $\alpha = 0^\circ$, the emitted light leaks into the substrate and air regions and does not propagate in the film, since there is no dispersion curve for $\hbar\omega < 2.85$ eV in Fig. 2(a). For $\alpha = 30^\circ$ and 60°, on the other hand, it can propagate in the film with nodes and antinodes of standing waves. The electric-field amplitude in the film is larger for $\alpha = 60^\circ$ than $\alpha = 30^\circ$, which is caused by the confinement of the electromagnetic energy due to the Fabry-Perot resonance. The larger amplitude is also a consequence of the compression of the electromagnetic energy density due to the small group velocity, which is equal to the energy velocity, for the case of $\alpha = 60^\circ$.

C. Numerical results for nanofibers

For the PWE calculation of dispersion curves of nanofibers, we took $L_x = L_y = 2.0$ μm and $N_\mathbf{G} = 33^2$ and we placed the thiacyanine fiber in the center of the supercell. Figure 7 shows the result of calculations for $\alpha = 30^\circ$ and 60°. There are multiple branches below the light line as thiacyanine films. The second lowest mode is inactive to fluorescence emission as before. We also confirmed that there was no mode below ω_T for $\alpha = 0^\circ$. That is the reason why in ideal J aggregates (Sec. I) effective propagation of fluorescence has never been reported.

Figure 8 shows the group refractive index of nanofibers obtained from the dispersion relation, but we did not evaluate

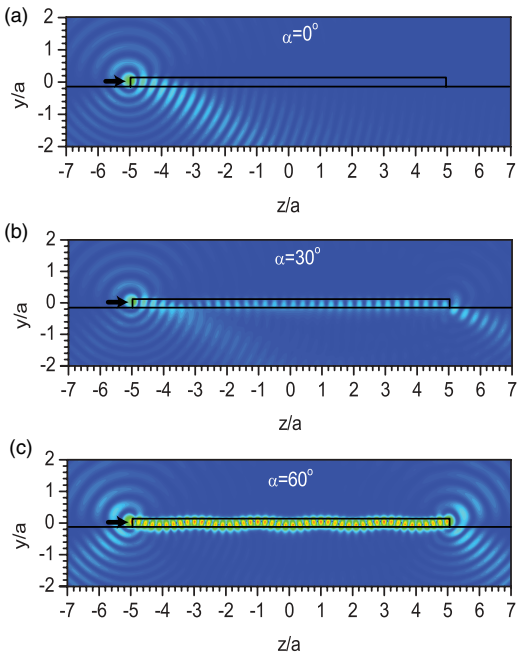

FIG. 6. (Color online) Electric-field distribution $|\mathbf{E}(y,z)|$ of light propagation in the thiacyanine film on the glass substrate for (a) $\alpha = 0^\circ$, (b) 30°, and (c) 60°.

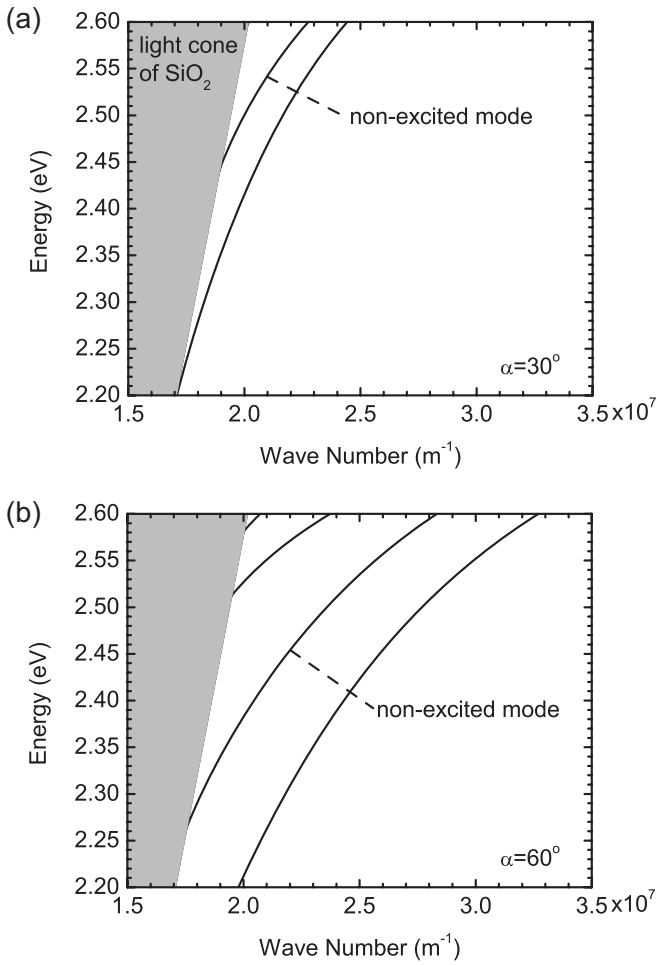

FIG. 7. Dispersion curves of the thiacyanine nanofiber for (a) $\alpha = 30^\circ$ and (b) 60°.

it by the FDTD method for this case, since it required a three-dimensional and time-consuming calculation. It is remarkable that the group index exceeds 12 even in the transparent frequency range below 2.6 eV for $\alpha = 60^\circ$.

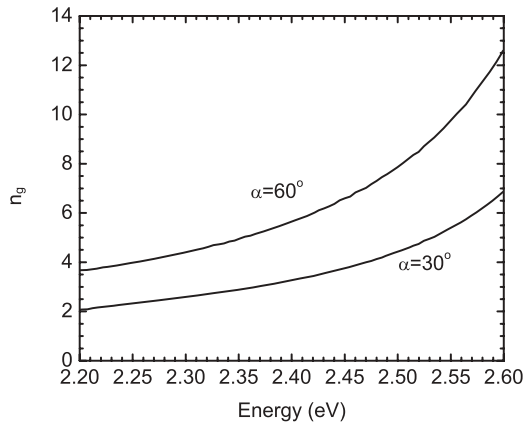

FIG. 8. Group refractive index of the nanofibers calculated by the PWE method.

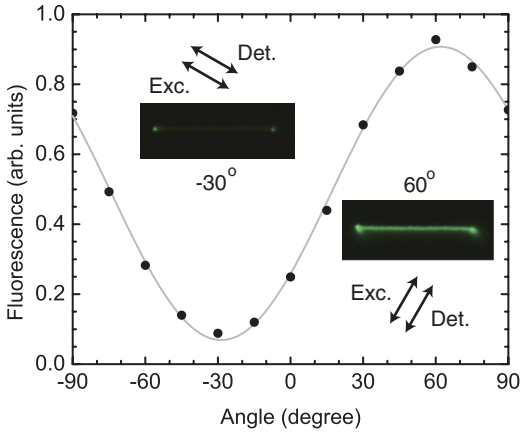

FIG. 9. (Color online) The dependence of the fluorescence intensity of the thiacyanine nanofiber on the polarization angle of the excitation light source. The direction of the polarizer, which is also the direction of the analyzer, is shown by a pair of arrows. Experimental data were provided by Takazawa.[25]

D. Comparison with experimental results

In this section, we show that our theoretical calculation can successfully explain the experimental results by properly choosing material parameters.

The tilt angle of the transition dipole moment of thiacyanine molecules in the nanofiber can be evaluated experimentally by observing the excitation polarization dependence of the fluorescence intensity, which is shown in Fig. 9.[25] The specimen was irradiated by a polarized light from a Hg lamp in the absorption band shown in Fig. 4. The polarization-angle dependence clearly shows a sinusoidal variation and it takes a maximum approximately at 60°. So, we assume that $\alpha = 60^\circ$ hereafter.

To examine ω_T and ω_L, we compared the reflection spectrum obtained by our calculation with that observed by Takazawa.[8] In the experimental study, he placed about 50 nanofibers on a glass substrate with random orientation and measured their reflection spectrum, which is shown in Fig. 10(a). There are two broad peaks around 3.1 and 2.5 eV. The former is close to the absorption peaks in Fig. 4, and the latter is close to the emission peak. The former peak can naturally be attributed to the polariton gap between ω_T and ω_L where the relevant component of the dielectric tensor is negative, while the latter peak originated from a limitation of the measurement facility that placed a monochromator between the specimen and the detector, so the fluorescence emission excited by shorter wavelength components of the input white light was observed as reflection.[8] Then, we calculated reflection spectra by assuming several combinations of ω_T and ω_L to reproduce the reflection peak around 3.1 eV. Because of the random orientation of the nanofibers, we used Eq. (7) for the dielectric tensor. The specular reflectance was calculated by assuming an unpolarized plane-wave input from the positive y direction in Fig. 1(a). A strong reflection is expected in the polariton gap between ω_T and ω_L. An optimized spectrum thus calculated is shown in Fig. 10(b), where $\hbar\omega_T$ and $\hbar\omega_L$ were assumed to be 2.85 and 3.2 eV, respectively. As will be described in the next paragraph, this choice of ω_T and ω_L can well reproduce the group

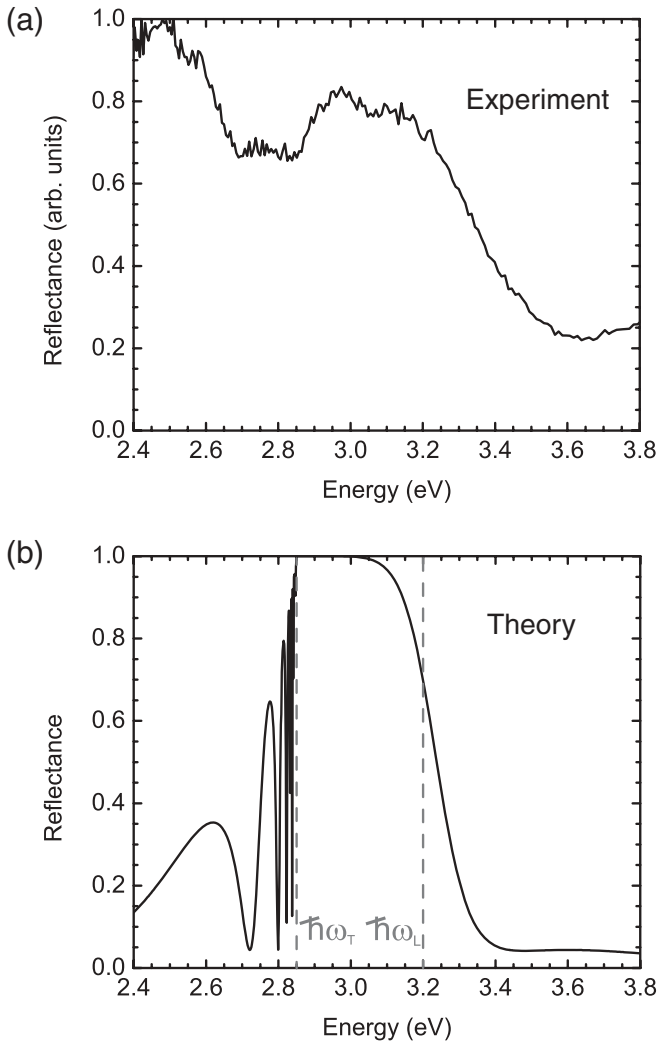

FIG. 10. (a) Experimental and (b) theoretical results of the reflectance of the thiacyanine nanofibers. To reproduce the reflection peak around 3.1 eV, $\hbar\omega_T$ and $\hbar\omega_L$ were assumed to be 2.85 and 3.2 eV, respectively. Experimental data were provided by Takazawa.[8]

refractive index found in Takazawa's experiment. Exciton polaritons in thiacyanine films and fibers are stable at room temperature, since their LT splitting is as large as 350 meV, which is approximately 12 times larger than the thermal energy (30 meV).

Figure 11 shows calculated and observed group indices, where the solid line is the same as Fig. 8 for $\alpha = 60^\circ$, and solid circles represent those values obtained from the Fabry-Perot interference peaks observed for nanofibers with various lengths. The interference peaks were measured with the fluorescence of thiacyanine molecules excited by a focused laser beam as a light source, so their measurement frequency range was limited by the fluorescence band, which is approximately from 2.2 to 2.7 eV as shown in Fig. 4. The measurement range was also limited by the absorption loss of the nanofiber, which was considerably large for $\hbar\omega > 2.55$ eV. So, the data are shown for 2.2 to 2.6 eV. Figure 11 shows a good agreement between the experimental observation and the theoretical calculation assuming $\hbar\omega_T = 2.85$ eV and $\hbar\omega_L = 3.2$ eV.

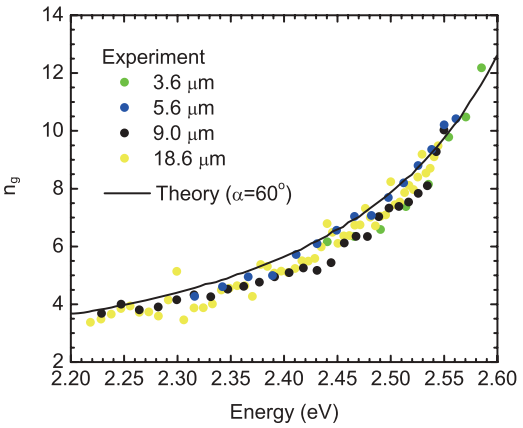

FIG. 11. (Color online) Theoretical (solid line) and experimental (solid circles) results of group refractive indices. The measurement was done for nanofibers with four different lengths. Experimental data were provided by Takazawa.[8]

Let us make one remark here. In Ref. 8, the interference pattern was analyzed not with the group refractive index but with the phase refractive index given by ck_z/ω, which led to an overestimation of the LT splitting. Moreover, $\hbar\omega_L$ was estimated at 3.64 eV from a minimum of the reflection spectrum. This energy is apparently higher than the upper edge of the broad reflection peak, which is expected to be close to $\hbar\omega_L$ from the calculation of the reflectance given in this paper.

In actual thiacyanine nanofiber specimens, h and w ranged from 100 to 200 nm and from 400 to 600 nm, respectively. So, we calculated dispersion curves assuming $\Delta h = \pm 50$ nm for $w = 500$ nm and $\Delta w = \pm 100$ nm for $h = 150$ nm. We found that the lowest dispersion curve shifted by $\Delta k_z \approx 10^6$ m^{-1} to the right (left) with increasing (decreasing) cross section, $w \times h$, in Fig. 7(b). However, the slope of the dispersion curve did not change appreciably, which can explain the relatively narrow distribution of n_g among four different specimens in Fig. 11.

In Ref. 26, Bragg gratings were introduced to thiacyanine nanofibers along the fiber axis by direct electron-beam writing. Then, a stop band with relatively high reflectivity was observed in each specimen, whose frequency was dependent on the period of the grating, Λ. Because the stop band was created by coherent multiple scattering, there is the following relation between Λ and the wave number of the first-order stop band: $k_z \approx \pi/\Lambda$. If we assume that the modification of the refractive index due to the grating is not so large, the frequency of the stop band is approximately given by the frequency of the dispersion curve at $k_z = \pi/\Lambda$. It was reported in Ref. 26 that the wavelength of the stop band was 560 nm ($\hbar\omega = 2.21$ eV) for $\Lambda = 160$ nm ($k_z = 1.96 \times 10^7$ m^{-1}). These values are very close to the lowest dispersion curve in Fig. 7(b), which gives another evidence of the accuracy of our calculation.

Finally, we point out the differences in exciton polaritons between organic-dye nanofibers and inorganic semiconductor nanowires. In ZnO nanowires,[16,17] clear Fabry-Perot peaks resulting from exciton polaritons can also be observed at room temperature. However, since original contrasts of refractive

indices of these semiconductors nanowires and substrates are large, light is confined even without effects of exciton polaritons. In other words, strong light confinement results not only from exciton polaritons but also from the total internal reflection due to large contrasts of refractive indices. In organic-dye nanofibers, on the other hand, strong light confinement results only from exciton polaritons, since in this paper refractive indices of organic-dye nanofibers and substrates are assumed to be the same ($\varepsilon_\infty = \varepsilon_{SiO_2} = 2.34$). It is surprising that group refractive indices of organic-dye nanofibers nevertheless exceed 12.

IV. CONCLUSIONS

To analyze the exciton-polariton dispersion relation of highly anisotropic thiacyanine films and nanofibers, we formulated a PWE method with the supercell technique that can calculate the eigenfrequencies as eigenvalues of a non-Hermitian matrix whose elements do not depend on frequency. We also analyzed the wave propagation in the film by the FDTD method. The group refractive index obtained from the slope of the dispersion curve agreed quite well with that obtained from the spacing of Fabry-Perot interference peaks in the transmission spectra. This agreement of the two independent calculations gives evidence of the accuracy of our calculation. In addition, we compared the reflection spectrum calculated for a thiacyanine film with an observed spectrum to estimate the transverse (ω_T) and longitudinal (ω_L) exciton frequencies at 2.85 and 3.2 eV, respectively.

We found that exciton polaritons of the Frenkel type in anisotropic films and fibers were quite different from isotropic ones. The number of polariton branches was infinite in the former due to the presence of diagonal elements with opposite signs in the anisotropic dielectric tensor. Moreover, the polariton dispersion relation strongly depended on the tilt angle α of the optical transition dipole moment of the constituent molecules to the propagation direction. By assuming $\alpha = 60^\circ$, we could reproduce quite well the group refractive index observed for thiacyanine nanofibers with various lengths. This value of the tilt angle was consistent with the experimental observation of the excitation-polarization dependence of the fluorescence intensity of the nanofibers. We also found that the effective single-mode frequency range was widened by the small coupling between the second lowest polariton branch and the electromagnetic field excited by the fluorescence of thiacyanine molecules, which resulted in the clear observation of a group index larger than 12 in a high frequency range close to ω_T.

ACKNOWLEDGMENT

We are grateful to Ken Takazawa for providing us with his experimental data and for valuable discussion on his specimens and experiments.

APPENDIX A: DERIVATION OF EQ. (16)

Substituting Eqs. (10), (11), (14), and (15) into Eqs. (12) and (13) yields the following matrix equations:

$$-\sum_{\mathbf{G}',\lambda}\eta^{-1}_{\mathbf{G}-\mathbf{G}'}(\mathbf{k}+\mathbf{G})\times\left[(\mathbf{k}+\mathbf{G})\times\mathbf{e}^{(\lambda)}_{\mathbf{k}+\mathbf{G}'}\right]D^{(\lambda)}_{n\mathbf{k}}(\mathbf{G}') + \sum_{\mathbf{G}'}\eta^{-1}_{\mathbf{G}-\mathbf{G}'}(\mathbf{k}+\mathbf{G})\times[(\mathbf{k}+\mathbf{G})\times\mathbf{n}]P_{n\mathbf{k}}(\mathbf{G}') = \frac{\omega^2_{n\mathbf{k}}}{c^2}\sum_{\lambda=1}^{2}D^{(\lambda)}_{n\mathbf{k}}(\mathbf{G})\mathbf{e}^{(\lambda)}_{\mathbf{k}+\mathbf{G}}, \tag{A1}$$

$$-2\sum_{\mathbf{G}',\lambda}\zeta_{\mathbf{G}-\mathbf{G}'}\mathbf{n}\cdot\mathbf{e}^{(\lambda)}_{\mathbf{k}+\mathbf{G}'}D^{(\lambda)}_{n\mathbf{k}}(\mathbf{G}') + \frac{\omega_T^2}{c^2}P_{n\mathbf{k}}(\mathbf{G}) + 2\sum_{\mathbf{G}'}\zeta_{\mathbf{G}-\mathbf{G}'}P_{n\mathbf{k}}(\mathbf{G}') = \frac{\omega^2_{n\mathbf{k}}}{c^2}P_{n\mathbf{k}}(\mathbf{G}), \tag{A2}$$

where

$$\zeta_{\mathbf{G}-\mathbf{G}'} = \sum_{\mathbf{G}''}\xi_{\mathbf{G}-\mathbf{G}''}\eta^{-1}_{\mathbf{G}''-\mathbf{G}'} \tag{A3}$$

and $\eta^{-1}_{\mathbf{G}-\mathbf{G}'}$ is the $(\mathbf{G},\mathbf{G}')$ element of the inverse of an $N_\mathbf{G}$-dimensional matrix whose $(\mathbf{G},\mathbf{G}')$ element is $\eta_{\mathbf{G}-\mathbf{G}'}$. Taking the inner product of $\mathbf{e}^{(1),(2)}_{\mathbf{k}+\mathbf{G}}$ and Eq. (A1), we obtain

$$\sum_{\mathbf{G}'}\mathbf{M}^{(\mathbf{k})}_{DD}(\mathbf{G},\mathbf{G}')\begin{bmatrix}D^{(1)}_{n\mathbf{k}}(\mathbf{G}')\\D^{(2)}_{n\mathbf{k}}(\mathbf{G}')\end{bmatrix} + \sum_{\mathbf{G}'}\mathbf{M}^{(\mathbf{k})}_{DP}(\mathbf{G},\mathbf{G}')P_{n\mathbf{k}}(\mathbf{G}') = \frac{\omega^2_{n\mathbf{k}}}{c^2}\begin{bmatrix}D^{(1)}_{n\mathbf{k}}(\mathbf{G})\\D^{(2)}_{n\mathbf{k}}(\mathbf{G})\end{bmatrix}, \tag{A4}$$

$$\sum_{\mathbf{G}'}\mathbf{M}^{(\mathbf{k})}_{PD}(\mathbf{G},\mathbf{G}')\begin{bmatrix}D^{(1)}_{n\mathbf{k}}(\mathbf{G}')\\D^{(2)}_{n\mathbf{k}}(\mathbf{G}')\end{bmatrix} + \sum_{\mathbf{G}'}\mathbf{M}^{(\mathbf{k})}_{PP}(\mathbf{G},\mathbf{G}')P_{n\mathbf{k}}(\mathbf{G}') = \frac{\omega^2_{n\mathbf{k}}}{c^2}P_{n\mathbf{k}}(\mathbf{G}). \tag{A5}$$

In Eqs. (A4) and (A5),

$$\mathbf{M}^{(\mathbf{k})}_{DD}(\mathbf{G},\mathbf{G}') = \eta^{-1}_{\mathbf{G}-\mathbf{G}'}|\mathbf{k}+\mathbf{G}|^2\begin{bmatrix}\mathbf{e}^{(1)}_{\mathbf{k}+\mathbf{G}}\cdot\mathbf{e}^{(1)}_{\mathbf{k}+\mathbf{G}'} & \mathbf{e}^{(1)}_{\mathbf{k}+\mathbf{G}}\cdot\mathbf{e}^{(2)}_{\mathbf{k}+\mathbf{G}'}\\ \mathbf{e}^{(2)}_{\mathbf{k}+\mathbf{G}}\cdot\mathbf{e}^{(1)}_{\mathbf{k}+\mathbf{G}'} & \mathbf{e}^{(2)}_{\mathbf{k}+\mathbf{G}}\cdot\mathbf{e}^{(2)}_{\mathbf{k}+\mathbf{G}'}\end{bmatrix}, \tag{A6}$$

$$\mathbf{M}^{(\mathbf{k})}_{DP}(\mathbf{G},\mathbf{G}') = -\eta^{-1}_{\mathbf{G}-\mathbf{G}'}|\mathbf{k}+\mathbf{G}|^2\begin{bmatrix}\mathbf{n}\cdot\mathbf{e}^{(1)}_{\mathbf{k}+\mathbf{G}}\\ \mathbf{n}\cdot\mathbf{e}^{(2)}_{\mathbf{k}+\mathbf{G}}\end{bmatrix}, \tag{A7}$$

$$\mathbf{M}^{(\mathbf{k})}_{PD}(\mathbf{G},\mathbf{G}') = -2\zeta_{\mathbf{G}-\mathbf{G}'}\left[\mathbf{n}\cdot\mathbf{e}^{(1)}_{\mathbf{k}+\mathbf{G}'}\ \mathbf{n}\cdot\mathbf{e}^{(2)}_{\mathbf{k}+\mathbf{G}'}\right], \tag{A8}$$

$$\mathbf{M}^{(\mathbf{k})}_{PP}(\mathbf{G},\mathbf{G}') = \frac{\omega_T^2}{c^2}\delta_{\mathbf{G},\mathbf{G}'} + 2\zeta_{\mathbf{G}-\mathbf{G}'}, \tag{A9}$$

where $\delta_{\mathbf{G},\mathbf{G}'}$ is Kronecker's delta and $\mathbf{M}^{(\mathbf{k})}_{ij}(\mathbf{G},\mathbf{G}')$ $(i,j = D,P)$ is the $(\mathbf{G},\mathbf{G}')$ element of the coefficient matrix $\mathbf{M}^{(\mathbf{k})}_{ij}$ in Eq. (16).

APPENDIX B: NUMBER OF DISPERSION CURVES

We examine the number of dispersion curves that should appear in Fig. 2. Let us consider the simplest case here, that is, Fig. 2(a), for which $\alpha = 0^\circ$ and the polariton modes are

all transverse magnetic. So, the magnetic field only has the x component, which we denote by H_x. It satisfies the following wave equation in the film ($|y| \leqslant h/2$):

$$-\frac{1}{\varepsilon_{zz}(\omega)}\frac{\partial^2 H_x(y,z)}{\partial y^2}-\frac{1}{\varepsilon_{yy}(\omega)}\frac{\partial^2 H_x(y,z)}{\partial z^2}=\frac{\omega^2}{c^2}H_x(y,z). \tag{B1}$$

Because the dielectric tensor is uniform in the film, H_x should be proportional to $\exp\{i(k_y y + k_z z)\}$. (Note that k_y can be imaginary.) Substituting H_x into Eq. (B1), we obtain

$$k_y^2=\varepsilon_{zz}(\omega)\left[\frac{\omega^2}{c^2}-\frac{k_z^2}{\varepsilon_{yy}(\omega)}\right]. \tag{B2}$$

According to the sign of k_y^2, there are two cases:

$$H_x(y,z)=\begin{cases} e^{ik_z z}[A\sin(k_y y)+B\cos(k_y y)] & \left(k_y^2>0\right) \\ e^{ik_z z}[Ae^{|k_y|y}+Be^{-|k_y|y}] & \left(k_y^2<0\right)\end{cases}, \tag{B3}$$

where two coefficients, A and B, are determined by the boundary conditions at $y=\pm h/2$.

For isotropic exciton polaritons, $\varepsilon_{xx}(\omega)=\varepsilon_{yy}(\omega)=\varepsilon_{zz}(\omega)<0$ for $\omega_T<\omega<\omega_L$. So, in this frequency range where there are surface modes, $k_y^2=\varepsilon_{zz}(\omega^2/c^2)-k_z^2<0$. Therefore, the y dependence of H_x is exponential with a real argument, which corresponds to conventional coupled surface polaritons.

For the anisotropic dielectric tensor given by Eq. (6), on the other hand, $\varepsilon_{xx}(\omega)=\varepsilon_{yy}(\omega)=\varepsilon_\infty$ and $\varepsilon_{zz}(\omega)=\varepsilon_\infty(2\omega_L^2-\omega_T^2-\omega^2)/(\omega_T^2-\omega^2)$. Because $\omega^2/c^2<k_z^2/\varepsilon_\infty$ below the light line,

$$k_y^2=\varepsilon_{zz}(\omega)\left[(\omega^2/c^2)-\left(k_z^2/\varepsilon_\infty\right)\right]>0 \tag{B4}$$

for $\varepsilon_{zz}(\omega)<0$. Then, k_y is real and the y dependence of H_x is sinusoidal in the film. For a given k_z, k_y^2 diverges to positive infinity when ω approaches ω_T from the positive side, since ε_{zz} diverges to negative infinity. So, there are an infinite number of modes, each of which is characterized by a different number of nodes.

[1] W. S. C. Chang, *Fundamentals of Guided-Wave Optoelectronic Devices* (Cambridge University Press, New York, 2010).
[2] G. Gantzounis and N. Stefanou, Phys. Rev. B **74**, 085102 (2006), and references therein.
[3] J. D. Joannopoulos, S. G. Johnson, J. N. Winn, and R. D. Meade, *Photonic Crystals: Molding the Flow of Light*, 2nd ed. (Princeton University Press, Princeton, NJ, 2008).
[4] S. A. Maier, *Plasmonics: Fundamentals and Applications* (Springer, Berlin, 2007).
[5] K. Takazawa, J. Phys. Chem. C **111**, 8671 (2007).
[6] K. Takazawa, Chem. Mater. **19**, 5293 (2007).
[7] K. Takazawa, Chem. Phys. Lett. **452**, 168 (2008).
[8] K. Takazawa, J. Inoue, K. Mitsuishi, and T. Takamasu, Phys. Rev. Lett. **105**, 067401 (2010).
[9] J. J. Hopfield, Phys. Rev. **112**, 1555 (1958).
[10] R. G. Ulbrich and G. W. Fehrenbach, Phys. Rev. Lett. **43**, 963 (1979).
[11] S. Chu and S. Wong, Phys. Rev. Lett. **48**, 738 (1982).
[12] A. Trichet, L. Sun, G. Pavlovic, N. A. Gippius, G. Malpuech, W. Xie, Z. Chen, M. Richard, and L. S. Dang, Phys. Rev. B **83**, 041302(R) (2011).
[13] J. R. Chen, T. C. Lu, Y. C. Wu, S. C. Lin, W. F. Hsieh, S. C. Wang, and H. Deng, Opt. Express **19**, 4101 (2011).
[14] S. Zhang, W. Xie, H. Dong, L. Sun, Y. Ling, J. Lu, Y. Duan, W. Shen, X. Shen, and Z. Chen, Appl. Phys. Lett. **100**, 101912 (2012).
[15] T. C. Lu, Y. Y. Lai, Y. P. Lan, S. W. Huang, J. R. Chen, Y. C. Wu, W. F. Hsieh, and H. Deng, Opt. Express **20**, 5530 (2012).
[16] L. K. van Vugt, S. Rühle, P. Ravindran, H. C. Gerritsen, L. Kuipers, and D. Vanmaekelbergh, Phys. Rev. Lett. **97**, 147401 (2006).
[17] S. Rühle, L. K. van Vugt, H.-Y. Li, N. A. Keizer, L. Kuipers, and D. Vanmaekelbergh, Nano Lett. **8**, 119 (2008).
[18] G. C. La Rocca, Nat. Photonics **4**, 343 (2010).
[19] S. Kena-Cohen and S. R. Forrest, Nat. Photonics **4**, 371 (2010).
[20] T. Ellenbogen, P. Steinvurzel, and K. B. Crozier, Appl. Phys. Lett. **98**, 261103 (2011).
[21] T. Ellenbogen and K. B. Crozier, Phys. Rev. B **84**, 161304(R) (2011).
[22] F. Würthner, T. E. Kaiser, and C. R. Saha-Möller, Angew. Chem. **50**, 3376 (2011).
[23] A. Taflove and S. C. Hagness, *Computational Electrodynamics: The Finite-Difference Time-Domain Method*, 3rd ed. (Artech House, Boston, 2005).
[24] W. Barford, *Electronic and Optical Properties of Conjugated Polymers* (Oxford University Press, New York, 2005).
[25] K. Takazawa (unpublished).
[26] K. Takazawa, K. Mitsuishi, and J. Inoue, Appl. Phys. Lett. **99**, 253302 (2011).